oceans

MDPI

*Communication*

# A Millennium-Scale Iberian Margin Chronology Validates the 1755 Lisbon Tsunami Record and Reveals Faro Record

**Fatima Abrantes [1,2,*], Sandra Gomes [1,3], Marta Salvado [2], Vitor Magalhães [1,4], Emilia Salgueiro [1,2], Teresa Drago [1,4], Livia Cordeiro [1,2] and Filipa Naughton [1,2]**

[1] Instituto Português do Mar e da Atmosfera—IPMA, 1495-165 Algés, Portugal; vitor.magalhaes@ipma.pt (V.M.); emilia.salgueiro@ipma.pt (E.S.); tdrago@ipma.pt (T.D.); livia.gebara@ipma.pt (L.C.); filipa.naughton@ipma.pt (F.N.)
[2] Centro de Ciências do Mar do Algarve—CCMAR/CIMAR, Universidade do Algarve, 8005-139 Faro, Portugal
[3] Unité Peuplements Végétaux et Bioagresseurs en Milieu Tropical—UMR PVBMT, Université de La Réunion, 97410 Saint Pierre, France
[4] Instituto Dom Luiz, Faculdade de Ciências, Universidade de Lisboa, 1749-016 Lisbon, Portugal
* Correspondence: fatima.abrantes@ipma.pt

**Abstract**

This work presents new data and several age–depth reconstructions based on distinct approaches to improve previously published age models for sedimentary sequences collected on the Iberian Margin middle shelf: PO287 6-1B, 2G (Porto); PO287 26-1B, 3G, and D13902 (Lisbon); and POPEI VC2B (Algarve). The new age models are constructed using radiocarbon dates calibrated with the IntCal20 calibration curve and smooth-spline regressions from the CLAM (non-Bayesian) and Bacon (Bayesian) models. A comparison of the age–depth models generated by the different approaches shows that, beyond the distinct solutions produced by CLAM and Bacon for each site, the differences between the two methods are inconsistent across sites. Furthermore, neither model yielded reliable results for the discontinuous sedimentary sequence with reworked older sediments and a hiatus. In this specific case, the "classical" linear regression (best-fit) approach appears to yield the results that enable intercomparison across all sequences. This exercise confirms the record of the 1755 earthquake and tsunami in the Lisbon core splice and a potential record of the same event in the Eastern Algarve, although the collected data indicate a more distal or lower-energy wave deposit.

**Keywords:** age model; Iberian Margin; last millennium; 1755 Lisbon earthquake and tsunami



Academic Editor: Beatriz Morales-Nin

Received: 20 May 2026
Revised: 11 June 2026
Accepted: 6 July 2026
Published: 10 July 2026



## 1. Introduction

Understanding the impact of climate warming on coastal upwelling systems, given their role as major drivers of primary production and their support for a significant share of global fisheries and climate regulation, is a priority [1]. However, many studies based on instrumental data and numerical models report both increases and decreases in upwelling intensity across locations, and even within the same location, which may reflect strong regional variability but leaves uncertainty about future evolution [2,3].

The western Iberian Margin (IM) marks the northern limit of the Canary upwelling system and is therefore a seasonally active upwelling region with high biological productivity [4,5]. Furthermore, areas of high sedimentation rates on the IM middle shelf are considered key to assessing changes in primary production and climate beyond the instrumental record [6]. The ICW3P project objective is to assess primary production and ecological variation over the past 1000 years, which, in Northern Europe, encompassed the Medieval Warm Period (also designated the Medieval Climate Anomaly, 950–1350 AD/CE), the cold Little Ice Age (1450–1850 AD/CE), and the Industrial Era (post 1850 AD/CE) (e.g., [7]). This project uses both classical and emerging proxies to provide an unequivocal record of the upwelling system's response to post-1850 AD/CE industrial warming. To document climate-driven changes, it is essential to consider the natural processes that may have influenced the sedimentary record in this region, particularly in the Lisbon area, which has experienced several major earthquakes (e.g., 1531, 1699, 1755), many of which were associated with tsunamis (e.g., [7]). Among these, the 1755 earthquake (Mw 8.75–9.0) and its transatlantic tsunami stand out as the most catastrophic, affecting at least 52 locations, although the 1531 event may have caused greater local damage in Lisbon. Historical, modeling, and geological evidence indicate significant tsunami impacts, especially in 1755, with run-up heights reaching 12–15 m in Lisbon and up to 30 m in the Algarve [7]. Sedimentary and geomorphologic evidence of tsunami inundation is preserved both onshore (e.g., [8–10]) and offshore, with tsunamite deposits and hiatuses described off Lisbon by Abrantes et al. [11,12]. This description was based on a comparison of magnetic susceptibility (MS), Anhysteretic remanent magnetization (ARM) in magnetite grains, Fe, mean grain size, $CaCO_3$ abundance, and radiocarbon chronology along the existing records from the Western Tagus System on the Portuguese continental shelf off Lisbon, including cores PO287 26-1B, 3G, and D13902. Those analyses identified anomalous event layers within the studied sedimentary sequences. A hiatus representing ~355 years of sedimentation and thicker instantaneous deposits—a 39 cm coarse unit with shell debris at the SSW site and a 1.5 m fine-grained unit at the W site (GeoB8903)—are interpreted as tsunamigenic features likely associated with the 1755 Lisbon earthquake. These results indicate contrasting depositional processes between sites, with higher-energy backwash conditions at the SSW location and preferential settling of fine suspended material at the W site. Together, they highlight the spatial variability of tsunami-driven sedimentation, while the synchronicity of their records provides key stratigraphic markers for regional correlation. As such, robust age models are needed for reliable temporal reconstructions, and consistency in their definition is especially critical for correlations between sedimentary sequences, because reconstructing past conditions, whether ecological, oceanographic, or climatic, depends on the assigned ages [13]. This prompted us to revisit and refine previously published age models for key sedimentary records from the Iberian Margin, including the Tagus site [11,12], the Porto record [14], and the Algarve sequence off Faro (POPEI VC2B), all of which were integrated in [6].

The objective of this brief communication is to present new data and methodologies to identify the most robust and consistent chronological framework for comparing the three sites studied, thereby underpinning the interpretation of the remaining ecological and oceanographic reconstructions of upwelling, primary production, and ecological variability over the last millennium as part of the ICW3P project.

## 2. Materials and Methods

The cores selected for this study are distributed by three regions of the Portuguese margin: the northwest—PO287 6-1B, 2G (Porto); the central region splice of PO287 26-1B, 3G, and D13902 (Lisbon); and the southern coast—POPEI VC2B (Algarve). All three sedimentary sequences have been previously analyzed and published by [6] (Table 1, Figure 1).

**Table 1.** ID, water depth, geographic location, core type, length, sampling cruise, date of recovery, sedimentation rate (SR), and age model origin of the sedimentary sequences used in the ICW3P study.

| Site ID | Core ID | Water Depth | Lat N | Long W | Core Type | Length | Ship–Cruise | Date | SR | Initial Age Model |
|---|---|---|---|---|---|---|---|---|---|---|
| | | (m) | | | | (m) | | | (mm yr$^{-1}$) | |
| Porto | PO287 6-1B, 2G | 84 | 41.3356 | 8.9888 | B-Box/ G-Gravity | 0.25/5.67 | RV Poseidon–PALEO1 | 2002 | 6.3 | Abrantes et al. (2011) [14] |
| Lisbon | D13902 | 90 | 38.5540 | 9.3355 | Long piston core | 6.00 | RV Discovery–249 | 2000 | 7.0 | Abrantes et al. (2005) [11] |
| Lisbon | PO287 26-1B, 3G | 96 | 38.5582 | 9.3640 | B-Box/ G-Gravity | 0.33/3.05 | RV Poseidon–PALEO1 | 2002 | 7.0 | Abrantes et al. (2005) [11] |
| Algarve | POPEI VC2B | 96 | 36.8800 | 8.0700 | Vibrocore | 1.81 | NRP Auriga–POPEI0108 | 2008 | 1.2 | Abrantes et al. (2017) [6] |

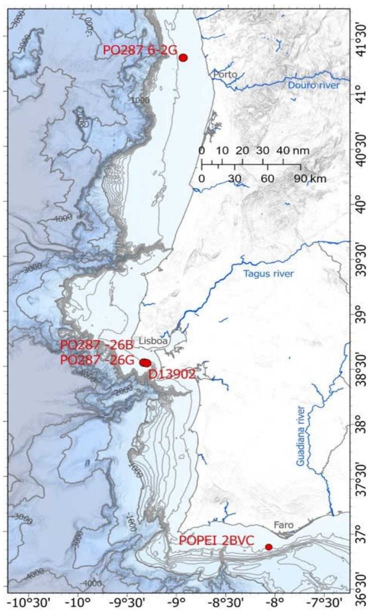


**Figure 1.** Geographic location of cores PO287 6-1B, 2G (Porto); PO287 26-1B, 3G, and D13902 (Lisbon); and POPEI VC2B (Algarve). Bathymetry from the GEBCO_2024 version.

The published age models for these cores were constructed using a combination of AMS$^{14}$C and $^{210}$Pb measurements from all box-cores and the top 50 cm of the long core retrieved from the same sites. (Table 2, [6,12]). Furthermore, we used a simple correlation between the magnetic susceptibility (MS) record obtained in the box-core and the long cores to better constrain the recovered top level of the long cores and to construct the spliced sequence for the Lisbon (PO287 26-1B, 3G gravity core, D13902 Piston core) and Porto (PO287 6-1B, 2G) sites [11].

**Table 2.** Conventional and 400-year reservoir-corrected AMS $^{14}$C BP dates for cores PO287 6-1B, 2G (Porto); PO287 26-1B, 3G, 13902 (Lisbon); and POPEI VC2B (Algarve). Numbers in bold correspond to new ages. Numbers in italic correspond to ages not considered in the best-fit age model approach.

| Lab ID | Original Depth | Spliced Depth | AMS 14C (yr BP) | AMS 14C (yr BP) w/Reservoir Correction | Error | Dated Material |
|---|---|---|---|---|---|---|
| | (cm) | (cm) | Conventional | | | |
| **PO287 6-1B** | | | | | | |
| *210Pb* | *0* | - | - | - | - | *2001/control* |

**Table 2.** *Cont.*

| Lab ID | Original Depth | Spliced Depth | AMS 14C (yr BP) | AMS 14C (yr BP) w/Reservoir Correction | Error | Dated Material |
|---|---|---|---|---|---|---|
| | (cm) | (cm) | Conventional | | | |
| *210Pb* | 20 | - | >1950 | - | 0 | 1950 6-1B, 20.7 cm/*control* |
| **PO287 6-2G** | | | | | | |
| AAR-8368.2-K | 51 | - | 440 | 40 | 25 | Shell in 26-1B/*control* |
| KIA 35149 | 100 | - | 560 | 160 | 25 | Mixed Forams (B) |
| ***KIA 58624*** | ***175*** | - | **1247** | ***847*** | ***27*** | ***Mixed Forams (P+B)*** |
| ***Beta 715417*** | ***205*** | - | **1150** | ***750*** | ***30*** | ***Mixed Forams (P+B)*** |
| ***Beta 715416*** | ***265*** | - | **1260** | ***860*** | ***30*** | ***Mixed Forams (P+B)*** |
| ***KIA 58625*** | ***275*** | - | **1214** | ***814*** | ***26*** | ***Mixed Forams (P+B)*** |
| *KIA 29290* | *317* | - | 805 | *405* | *35* | *Mixed Forams (P)* |
| KIA 35150 | 400 | - | 1220 | 820 | 30 | Mixed Forams (B) |
| **PO287 26-1B** | | | | | | |
| AAR-8368.2-K | 32–33 | 51–52 | 440 | 40 | 25 | Shell in 26-1B/*control* |
| **PO287 26-3G** | | | | | | |
| OS-42380 | 20–21 | 20 | 455 | 55 | 25 | Snail |
| OS-42381 | 86–87 | 86 | 545 | 145 | 25 | Snail |
| *KIA58629* | *88–90* | *88* | *1080* | *680* | *40* | *Mixed Forams (P)* |
| ***Beta 715418*** | ***94–95*** | ***94*** | **720** | ***320*** | **30** | **Mixed Forams (P+B)** |
| *KIA 23661* | *125–126* | *125* | 1310 | *910* | 25 | Snail |
| **Beta 715417** | **128–129** | **128** | **870** | **470** | **30** | **Mixed Forams (P+B)** |
| KIA58626 | 138–139 | 138 | 729 | 329 | 26 | Mixed Forams (P) |
| **PO287 26-1B** | | | | | | |
| AAR-8368.2-K | 32–33 | 51–52 | 440 | 40 | 25 | Shell in 26-1B/*control* |
| **D13902** | | | | | | |
| OS-37286 | 27–28 | 75.4–76.4 | 492 | 92 | 39 | Shell |
| *AAR-8338* | *31–32* | *79.4–80.4* | *2100* | *1700* | *80* | *Shell* |
| *AAR-7826* | *37–38* | *85.4–86.4* | *8955* | *8555* | *70* | *Shell* |
| *AAR-8301* | *46–47* | *94.5–95.4* | *7075* | *6675* | *50* | *Shell* |
| AAR-7207 | 62–63 | 110.4–111.4 | 1160 | 760 | 45 | Shell |
| AAR-7208 | 62–63 | 110.4–111.4 | 1185 | 785 | 40 | Turritela |
| AAR-7209 | 96–97 | 144.4–145.4 | 1370 | 970 | 45 | Shell |
| OS-37307 | 124–125 | 172.4–173.4 | 1880 | 1480 | 80 | Shell fragment |
| AAR-7828 | 151–152 | 199.4–200.4 | 2007 | 1607 | 37 | Shell |
| AAR-7826 | 199–200 | 247.4–248.4 | 2340 | 1940 | 55 | Shell |
| **POPEI** | | | | | | |
| *210Pb* | - | *0.00* | | - | - | *2008/control* |
| 210Pb | - | 29.58 | | - | - | *1951/control* |
| 210Pb | - | 40.11 | | - | - | *1876/control* |
| ***Beta758681*** | - | ***40.5*** | ***570*** | ***170*** | ***30*** | ***Mixed Forams (P+B)*** |
| ***Beta758679*** | - | ***50.5*** | ***610*** | ***210*** | ***30*** | ***Mixed Forams (P+B)*** |
| ***Beta758680*** | - | ***60.5*** | ***640*** | ***240*** | ***30*** | ***Mixed Forams (P+B)*** |
| ***Beta463037*** | - | ***78.22*** | ***740*** | ***340*** | ***30*** | ***Mixed Forams (P+B)*** |
| **KIA58627** | - | **90.25** | **948** | **548** | **27** | **Mixed Forams (P+B)** |
| Beta 715420 | - | 110.4 | 1440 | 1040 | 30 | Mixed Forams (P+B) |
| *Beta 278216* | - | *130.87* | *1220* | *820* | *40* | *Mollusk Shell* |
| ***KIA58628*** | - | ***175.40*** | ***1896*** | ***1496*** | ***27*** | ***Mollusk shell*** |
| OS-97152 | - | 200.57 | 2130 | 1730 | 25 | Mixed Forams (P+B) |
| Beta 715421 | - | 211.6 | 2160 | 1760 | 30 | Mixed Forams (P+B) |
| OS-97143 | - | 270.29 | 3020 | 2620 | 25 | Mixed Forams (P+B) |

Uncertainties in the $^{210}$Pb method arise from variable fluxes and mixing. We addressed this by using high sampling resolution for the box-core and the long core top, which also ensured that base activity determinations were reached. Furthermore, $^{210}$Pb data were combined with measurements of $^{137}$Cs and $^{226}$Ra. To verify the reliability of the date assigned to the box-core top, which is generally assumed to be the year before the recovery date, we have dated the box-core bottom using AMS$^{14}$C and calculated the top age using the sedimentation rate (SR) derived from the two topmost AMS$^{14}$C dates.

For AMS$^{14}$C, the main sources of uncertainty are geographic variability in reservoir effects, sample contamination from reworking, and calibration uncertainties (e.g., [15]). In our case, the reservoir effect at the Tagus site was measured at 400 ± 36 years, as reported by Abrantes et al. [11]. We consider this value appropriate for the continental shelf as a whole, particularly because it aligns with the most commonly used average. To avoid sample contamination, the dated material consisted only of mollusk shells, if found complete, in a living position and on an undisturbed level, or of planktonic foraminifera. Because all cores were retrieved between 80 and 90 m below sea level (mbsl), where planktonic foraminifera are generally scarce, the required number of specimens was obtained by combining planktonic species; at other levels, a mix of planktonic and benthic forms was required (Table 2). Although combining species from the pelagic and benthic environments may result in a mix of different ages, we believe that because the sites' depths lie above the maximum depth of light penetration and because the surface water masses typically extend down to 100 to 200 mbsl, this is not a concern. Furthermore, all foraminifera were carefully hand-picked and ultrasonicated before standard pre-treatments were performed by the measuring laboratories. As for calibration, the published models were calibrated using Intcal04.14c.

Additionally, we used MS measurements from box-cores and long cores collected in Bremen using a Multi-Sensor Core Logger (MSCL-S—Geotek Ltd., Daventry, UK). MS was measured at 3 cm intervals, making this proxy an effective tool for developing composite stratigraphic sections and aligning core sequences on a common depth scale. The reliability of the method is demonstrated by its widespread use to correlate sediments and stratigraphically align long cores, such as those collected by the International Ocean Discovery Program (IODP) [15]. We therefore anchored our dates to the MS-defined splices of the box and long cores at each site. MS has also enabled the identification of less-dated or more problematic intervals and the selection of new levels to be dated (Figure 2; Table 2 [6,11,12,14]).

Since the publication of the previous age–depth models based on linear regression (best-fit), updated IntCal20 and Marine20 calibration curves have been published [16,17]. For the historical period—the focus of this study—the IntCal14 and IntCal20 curves show similar trends. However, the IntCal20 achieves higher resolution for the recent millennia by incorporating tree-ring data that resolve $^{14}$C variations on sub-decadal to annual timescales. This improvement ensures that sharp, short-term events such as the so-called Miyake events, linked to intense solar activity around 775 AD/CE and 993–994 AD/CE [16], are faithfully represented in the calibration curve. In addition, the most recently published age–depth models are constructed using spline-based approaches (e.g., CLAM [18]) or Bayesian modeling frameworks such as OxCal [19] and Bacon [20]. Consequently, we revised our previously published age models using the CLAM and Bacon software, both developed by the same author and widely used for paleo reconstructions (e.g., [21]). Both approaches were applied to the age datasets from the three sites, using the respective R code packages (CLAM script and rbacon-Version 3.3.1), keeping in mind that CLAM is considered to respond better to sparse chronological data and to be more flexible in handling abrupt changes such as hiatuses [22], while Bacon is less responsive to abrupt changes but produces age estimates with the most appropriate uncertainty estimates and avoids age reversals [23].

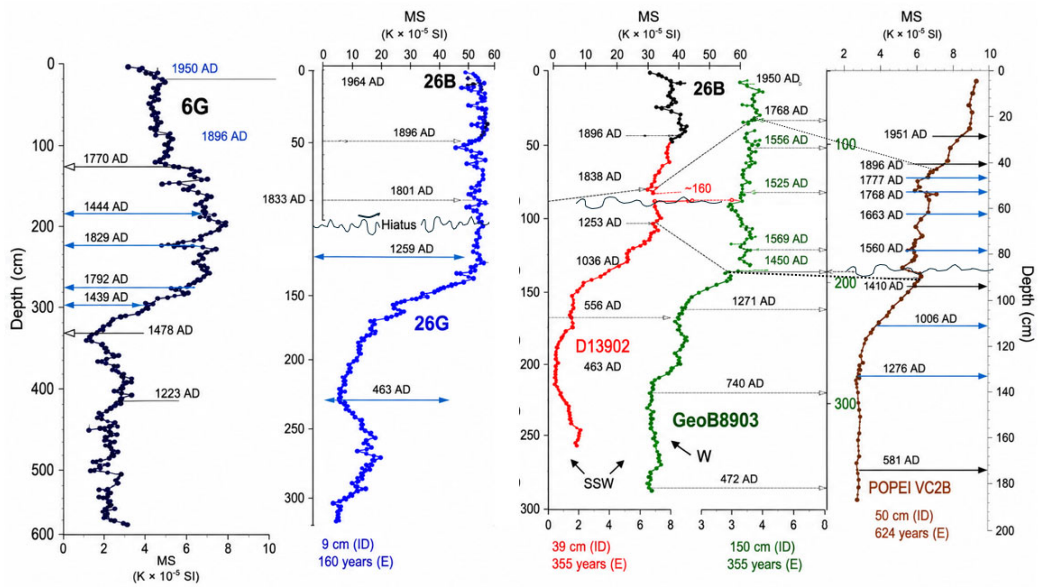


**Figure 2.** Depth vs. ages AD/CE on the magnetic susceptibility record of the Porto sequence (PO287 6-1B, 2G); the Lisbon sites (PO287 26-1B, 3G, D13902; GeoB8903); and the Algarve site (POPEI VC2B). Black arrows and associated numbers designate calibrated accelerator mass spectrometry 14C ages obtained for the respective core, and a wavy line indicates a hiatus. The red arrow and number 160 in core D13902 indicate that the magnetic susceptibility values at this level reach a maximum of 160 (see Abrantes et al. 2005 [11] for explanation). Black lines indicate features in the PO287 6-2G sequence that are correlated with either 26-3G, GeoB8903, or POPEI VC2B, showing ages transferred from these latter records into PO287 6-2G and POPEI VC2B. Blue lines correspond to new dated levels. SSW—cores located in the SSW area of the Tagus mouth; W—core located to the W of the Tagus mouth.

The $^{14}$C yr BP (BP: Before Present; present: 1950) data for all cores included in the ICW3P project are presented in Table 2. Radiocarbon dates were calibrated using IntCal20 after applying a 400-year reservoir-effect correction [11,12], and with $^{210}$Pb dates fixed as calendar anchor points. The use of IntCal20 was necessary because the MRAs incorporated into the Marine20 dataset allow calibration only for uncorrected AMS$^{14}$C dates of 603 $^{14}$C yr BP or older [16]. Given that the present study focuses on the last 1000 years, this restriction makes Marine20 impractical for the purposes cited above.

## 3. Results

### *3.1. Porto Site PO2876-1B, 2G*

A total of eight sediment levels have been dated, four of which (175, 205, 265, and 275 cm) are new dates (Table 2, Figure 2). Of these four levels, 175 and 275 cm were sent to the Leibniz Laboratory at Kiel University, but instrumental problems just before our measurements and uncertainty about possible measurements led to 205 and 265 cm being sent later to BetaAnalytics. Both Beta and KIA dates gave much older ages than the previously dated levels, both above 175 cm and below 275 cm. The new samples were composed of a mix of benthic and planktonic foraminifera, which makes clay cleaning difficult and can result in older ages, as shown by Ausin et al. (2021) [24]. Furthermore, unpublished data from a dating experiment at the Tagus site, conducted with Jan Heinemeier and the Aarhus University dating laboratory, including measurements for five levels done on four subsamples composed of *G. bulloides*, mixed planktonic, mixed benthic and planktonic, and total sediment, revealed that the mixed samples provided ages older than *G. bulloides* but younger than the total sediment, leading us to conclude that sonication of different species either breaks the most fragile or does not completely remove the clay material present within some other species. Given the objectives of CLAM and Bacon to utilize all available dates, the two models were run including all dates after IntCal20 was used for calibration. However, to reach an acceptable model, the new ages had to be excluded from all three different approaches.

Figure 3A compares the three age–depth models and suggests continuous sedimentation with no major discontinuities, but it also shows that Bacon and CLAM yield distinct solutions between 1000 and 1700 AD/CE, with Bacon estimating a higher sedimentation rate than CLAM.

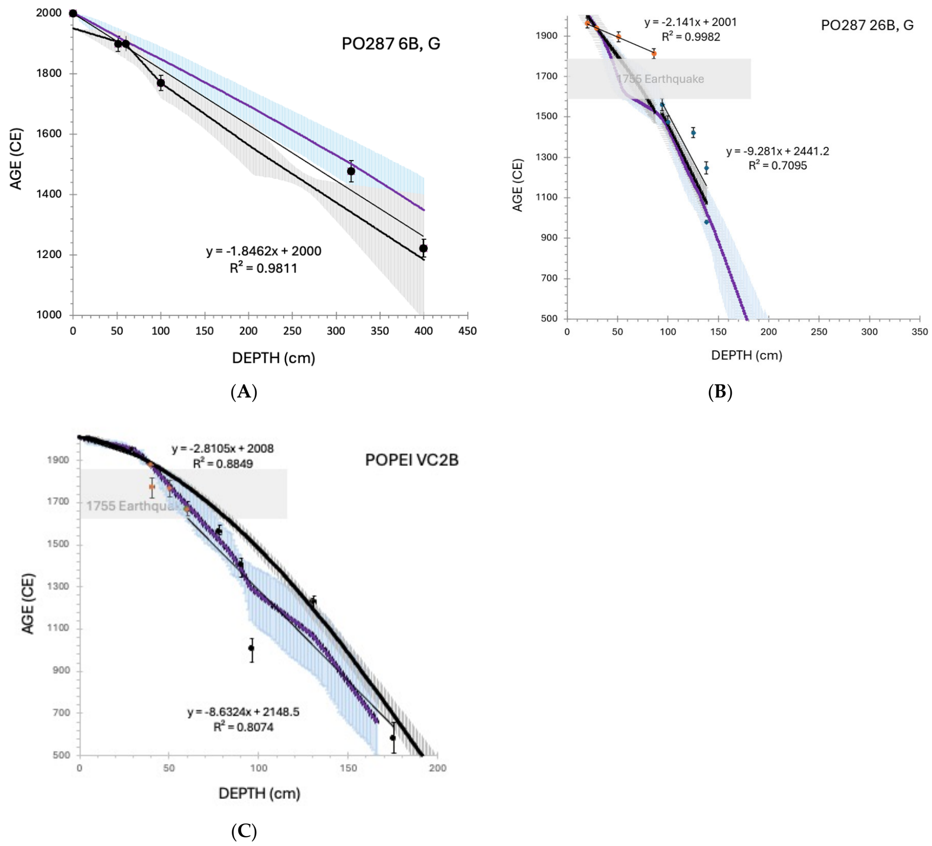


**Figure 3.** Age–depth model comparison showing CLAM (thick black), Bacon (violet), and traditional best-fit (thin black) curves. Gray- and blue-shaded areas indicate the 95% confidence intervals (uncertainty ranges) for the CLAM and Bacon models, respectively. (**A**) Porto splice of PO287 6-1B, 3G; (**B**) Lisbon splice of PO287 26-1B, 3G; (**C**) Core POPEI VC2B (Algarve).

### *3.2. Lisbon Splice PO287 26-1B, 3G, D13902*

The Lisbon sequence was already highly dated (16 levels), and two new levels (94 and 198 cm) were added in core PO287 26-3G (Figure 3B). Levels between 75 and 95 cm exhibit anomalous older values (Table 2, Figure 2) and were interpreted as representing allochthonous material transported into the area during the 1755 AD/CE Lisbon earthquake and tsunami [12].

Several attempts were made with the CLAM and Bacon runs, including imposing a hiatus, a slump, and finally retiring the older ages and running the models with the remaining ages. Neither CLAM nor Bacon yield reliable results when those levels are included, not even when hiatuses or slumps are imposed on the models. Only after removing the older ages do both models run without problems, but then the resulting curve is continuous, as shown in Figure 3B, which also reveals that all three approaches, CLAM, Bacon, and the best-fit model, provide closer ages below 100 cm, but are offset at the top.

### *3.3. Algarve POPEI VC2B*

The Algarve sequence (POPEI VC2B) was the least dated, and a mixture of planktonic and benthic foraminifera from six new levels was picked and prepared for AMS$^{14}$C dating (Table 2, Figure 2).

The $^{210}$Pb-derived and AMS$^{14}$C dates reveal a few intriguing aspects: 1) two levels 0.4 cm apart differ by 100 years in age; 2) AD/CE ages 1766 and 1774 (an 8-year difference) occur 10 cm apart at 40.5 to 50.5 cm, yielding an SR = 1.25 cm/yr; 3) the $^{210}$Pb model indicates an SR = 0.52 cm/yr [6]; and 4) AMS$^{14}$C dates between 175.40 and 90 cm yield an SR = 0.08 cm/yr, that is, a sedimentation rate about six times lower than in the upper section. All these features suggest anomalous sedimentation between 90 and 40 cm and a major change in sedimentation dynamics above 40 cm. An evaluation of how these age anomalies relate to the sediment's physical and chemical composition along the POPEI VC2B core was conducted using MS, XRF-determined Fe and Ca (as ln), and sand (w%) distribution (Figure 4). Although the MS record shows no marked change, aside from higher variability around a slight increasing tendency between 100 and 40 cm that interrupts the clear increasing tendency observed below 100 cm and above 40 cm, Fe and Ca are marked by sharp minima between 100 m and 92 cm, with the Ca minimum centered at 97 cm and the Fe minimum at 93 cm. Above 92 cm, both elements also show a rapid increase: Ca reaches a maximum at 90 cm, followed by a continuous decrease, while Fe shows a continuous increase up to 40 cm. Ca and Fe minima co-occur with a decrease in grain size (sand w%) that continues up to 40 cm. In the top 40 cm, Ca, Fe and sand records show variability around a constant mean. This combined information indicates a major change in sediment composition around 100–90 cm, followed by an initial deposit of ±6 cm of Ca-rich, silt-sized particles, and a subsequent decrease in Ca and an enrichment in silt-sized, Fe-rich, likely terrigenous particles.

Results from the CLAM and Bacon runs, including all existing dates and the best-fit model, are presented in Figure 3C. CLAM and Bacon provide continuous records but different solutions, with CLAM estimating higher sedimentation rates than Bacon, contrary to what is observed at the Porto site. However, based on the above-discussed intriguing sequence of AMS $^{14}$C dates (Table 2, Figure 2) and sediment composition, we defined a best-fit model split at 90.25–40.5 cm.

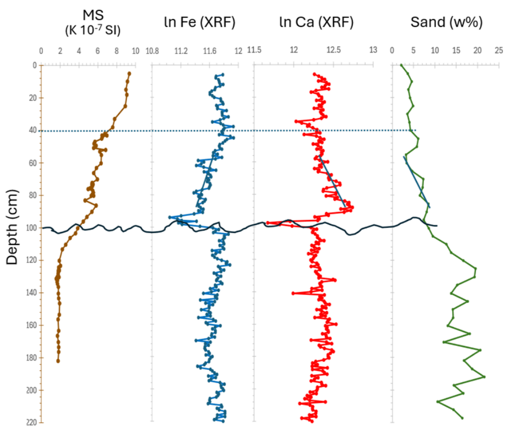


**Figure 4.** MS, XRF-determined Fe and Ca (as ln), and % sand along core POPEI VC2B. The wavy line indicates the hiatus level, while the dotted line marks the assumed top of the disturbed interval.

## 4. Discussion

The comparison of age–depth models across sites, based on distinct methods—CLAM, Bacon, and the classical best-fit approach—is shown in Figure 3A–C. These figures show that age models derived from the R software packages CLAM and Bacon did not account for the sequences with disturbed sediments. At the Lisbon site, AMS$^{14}$C ages of 7 to 9 ky (Table 2), associated with an obvious hiatus, were the primary evidence for the earthquake and tsunami record but were not resolved even when imposing a hiatus or a slump to the model. The only solution was to exclude the older ages, but then, the resulting model considered a continuous sedimentation rate (Figure 3B). Furthermore, as noted in comparisons of the two models by other authors, sedimentation rates are underestimated by CLAM but overestimated by Bacon (e.g., [25]). However, in our case, the differences observed between the two methods at both sites differ in sign between Porto and Algarve (Figure 3A–C). For these reasons, we decided to use linear regression of the dated levels, which provides a single best-fit line through radiometric ages, assuming a constant growth rate within the pre-defined depths, as in previously published models of these same sites. Although considered a "classical" method, mostly used before the Bayesian era, linear regression is a formal statistical model that remains relevant and is often used as a baseline or default age–depth modeling method, applied to a few dated points to produce age–depth models for the last millennium's records (e.g., [26–28]). Furthermore, as noted by [22], age–depth model selection must consider the sedimentological and stratigraphic context, as well as the study objectives, to ensure reliable reconstructions.

For the Porto and Lisbon sites, the new recalibrated age–depth models confirmed the previously established sedimentation dynamics. By contrast, the new AMS$^{14}$C-dated levels in the Algarve core revealed sedimentological anomalies that prompted an interpretation consistent with the one proposed to explain the record of a suite of seven cores collected off Faro and studied during the EU project ASTARTE along the eastern Algarve transect [29]. Likewise, Feist et al. (2023) [30] identified a relatively thin (20–40 cm) layer as event deposit Ez in cores located southwest of Faro, at about 8° 30 W. A thicker sediment layer on the upper shelf, down to 79 mbsl, that thins toward 111 mbsl is also attributed by the authors to the 1755 tsunami (Figure 5).

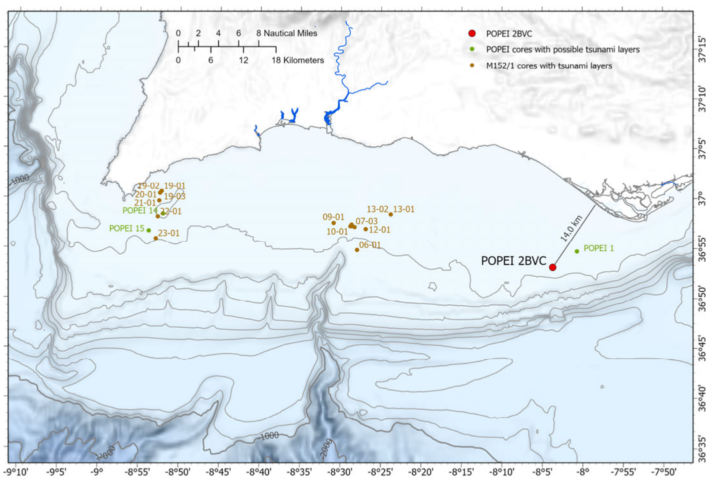


**Figure 5.** POPEI VC2B relative location to the ASTARTE and Feist et al., 2023 [30] studies of sedimentary sequences. Green dots indicate possible tsunami records. Brown dots indicate sedimentary sequences where tsunami records have been identified.

With this hypothesis in mind, the anomalous sequence between 100 and 40.5 cm (dated at levels 90.25 and 40.5 cm) likely represents a 50 cm instantaneous deposit of reworked material transported by the last, lower-energy waves during a tsunami. Assuming an SR of 0.08 cm/yr, the estimated date for the 100 cm level would be 1131 AD/CE, and the age difference between this level and the year of the tsunami (1755) indicates an erosion of 218 cm/624 years of record. If, on the other hand, the drastic increase in SR observed at the core top is assumed to propagate downcore between 40 and 100 cm, then 1755 AD/CE would be at 82.46 cm, that is, at the base of the disturbed interval.

Although the ongoing discussion about the potential source of the 1755 Lisbon earthquake and tsunami [31,32], the proposed locations also include the Portimão and Cadiz Faults to explain the destruction generated in the Alboran and eastern Algarve [33]. However, its dispersion and damage reached the Northern European coasts, North America, Brazil, and the Caribbean [34].

Offshore records are well documented not only off Lisbon [11,12] but also in remobilized sediment layers identified at three sites along the Gibraltar coast [35]. In the Algarve, the most severely affected area, the coast was also heavily impacted. Western areas were exposed directly to the tsunami's force, whereas sand barriers and lagoons between Faro and Tavira may have partially protected the hinterland. However, historical accounts included in the Inquiry ordered by the Marquis de Pombal, a survey sent to every parish in Portugal [36], describe Faro as largely destroyed by the earthquake and inundated by the tsunami:

"…forão lastimosos os estragos causados tanto pelo tremor, como pelo mar. Em poucos minutos foi vista a famosa Faro hum monte de ruinas, ella foi arrazada pelos fundamentos, raros edificios escaparão, estes ficarão moidos… A sua observancia foi perturbada pela voz, de que o mar sahia do seo curso, e vinha correndo a tragar a Cidade. Este segundo terror nos obrigou a abandonar tudo para salvar-mos as vidas nos altos imediatos com dobrado terror… O mar recolheo-se em partes mais de 20 braças, deixando as praias em secco; e arremetendo immediatamente para a terra com tamanho impeto que entrou por ella dentro mais de uma legua, sobrepujando as mais altas rochas; tornando a retrair-se e romper por três vezes dentro de poucos minutos, arrastando no fluxo e refluxo enormes massas de penhascos e edifícios; e deixando por isso arrazadas quase todas as povoações marítimas" [36].

Translation: … The damage caused by both the earthquake and the sea was lamentable. In a few minutes, the famous Faro was reduced to a pile of ruins; few buildings escaped; those that did were crushed… This observation was disturbed by the sound of the sea leaving its course and rushing to engulf the city. This second terror forced us to abandon everything to save our lives on the immediate heights, with doubled fear… the sea retreated in parts by more than 20 fathoms, leaving the beaches dry; it then rushed toward the land with such force that it penetrated more than a league inland, overtopping the highest rocks. It retreated and surged three times within a few minutes, dragging enormous masses of cliffs and buildings, leaving nearly all coastal settlements devastated.

Based on available data and descriptions from an additional, independent historical source—even accounting for exaggeration due to panic—it is evident that the POPEI VC2B location at 90 mbsl, approximately 14 km offshore, was affected by this episode. The combination of the AMS$^{14}$C dates and the diagnostic features (grain-size distribution and physical and chemical properties) that characterize the event in cores closer to the Tagus River mouth is less evident in the POPEI record, but suggests major erosion followed by the instantaneous input of terrigenous fine sediments (Figure 4). However, the lack of strong diagnostic features associated with fine-sediment deposition was also reported for the GeoB8903 core at 102 mbsl, to the west of the Tagus mouth, where fine sediments of approximately the same age were found over a ±150 cm thick interval [12].

Although these results have all the limitations associated with the model used to define the depth–age relationship at each site, they are corroborated by historical accounts describing three tsunami waves of progressively decreasing intensity. This Algarve sequence may account for the erosion of sediment and transport of coarser terrigenous materials by the initial, higher-energy wave farther offshore. In contrast, the subsequent, lower-energy waves—particularly at sites east of the main wave return path, which is apparently closer to the location studied by Feist et al. (2023) [30] (Figure 5)—likely reworked and redeposited surrounding sediments. Such processes could have led to the rapid accumulation of material with characteristics similar to those of the local background sediments. Although these findings indicate the removal of most of the sedimentary record corresponding to the Little Ice Age at both the Lisbon and Algarve sites, they do not preclude us from assessing primary production and ecological variation during the Medieval Climate Anomaly, nor from evaluating differences between that warm period and the post-1850 AD/CE warming.

## 5. Conclusions

This study underscores that age–depth model selection is not neutral and must be guided by the sedimentological meaning of age reversals, intervals with older ages, or other important changes in SR within the sequence. The accepted age–depth model determines the interpretation of past conditions, whether ecological, oceanographic, or climatic, or of the sequence of events behind disturbed deposits, such as the 1755 Lisbon tsunami.

Both CLAM and Bacon age–depth models appear not ideally suited to high-resolution, disturbed sedimentary sequences. Nonetheless, to ensure reliable inter-site comparisons, it is imperative to adopt a consistent methodology for constructing age models. Consequently, we employed a classical linear best-fit approach to establish a framework for more consistent comparison of all sedimentary sequences selected to reconstruct past environmental conditions using the various proxy datasets generated by the ICW3P project participants.

The new age models confirm the record of the 1755 earthquake and tsunami in the Lisbon core splice. Furthermore, the new evidence from the Algarve site is proposed to represent a hiatus, followed by deposition of an approximately 60 cm thick layer of nearly contemporaneous sediments. This deposit is interpreted as a distal, tsunami-derived signal associated with the final, lower-energy waves felt in the Eastern Algarve during the 1755 tsunami.

**Author Contributions:** Conceptualization, F.A.; Methodology, F.A., E.S., M.S., V.M., T.D. and L.C.; Software, S.G.; Validation, F.N., V.M. and S.G.; Data Curation, F.A. and V.M.; Writing—Original Draft Preparation, F.A.; Writing—Review and Editing, F.A., F.N., E.S., T.D., M.S. and V.M.; Project Administration, F.A. and L.C.; Funding Acquisition, F.A., E.S. and L.C. All authors have read and agreed to the published version of the manuscript.

**Funding:** Main funding was provided by the Fundação para a Ciência e Tecnologia (FCT) project PTDC/CTA-CLI/2884/2021—Impact of climate warming in the coastal upwelling system and primary production off Portugal: a study linking classical and emergent proxies (ICW3P). This study has also received Portuguese national funds from FCT—Foundation for Science and Technology, under UID/04326/2025 (DOI https://doi.org/10.54499/UID/04326/2025), UID/PRR/04326/2025 (DOI https://doi.org/10.54499/UID/PRR/04326/2025), and LA/P/0101/2020 (DOI https://doi.org/10.54499/LA/P/0101/2020), and from the operational program COMPETE 2020 through contract EMSO-PT FEDER-01/SAICT/2016.

**Data Availability Statement:** Data will be available at the PANGAEA—Data Publisher for Earth & Environmental Science (DOI to be provided at time of publication).

**Acknowledgments:** The authors thank Warley Soares for laboratory support at IPMA and the personnel in human resources, project management, and the financial section of CCMAR.

**Conflicts of Interest:** The authors declare no conflicts of interest.

## References

1. IPCC. Summary for Policymakers. In *IPCC Special Report on the Ocean and Cryosphere in a Changing Climate*; Pörtner, H.-O., Masson-Delmotte, D.C.R.V., Zhai, P., Tignor, M., Poloczanska, E., Mintenbeck, K., Alegría, A., Nicolai, M., Okem, A., Petzold, J., et al., Eds.; Cambridge University Press: Cambridge, UK; New York, NY, USA, 2020.
2. Bakun, A. Global Climate change and intensification of coastal ocean upweling. *Science* **1990**, *247*, 198–201. [CrossRef] [PubMed]
3. Wang, D.; Gouhier, T.C.; Menge, B.A.; Ganguly, A.R. Intensification and spatial homogenization of coastal upwelling under climate change. *Nature* **2015**, *518*, 390–394. [CrossRef] [PubMed]
4. Fiuza, A. Upwelling patterns off Portugal. In *Coastal Upwelling Its Sediment Record*, 1st ed.; Suess, E., Thiede, J., Eds.; Plenum: New York, NY, USA, 1983; Volume 1, pp. 85–98.
5. Abrantes, F.; Sancetta, C. Diatom assemblages in surface sediments reflect coastal upwelling off southern Portugal. *Oceanol. Acta* **1985**, *8*, 7–12.
6. Abrantes, F.; Rodrigues, T.; Rufino, M.; Salgueiro, E.; Oliveira, D.; Gomes, S.; Oliveira, P.; Costa, A.; Mil-Homens, M.; Drago, T.; et al. The climate of the Common Era off the Iberian Peninsula. *Clim. Past* **2017**, *13*, 1901–1918. [CrossRef]
7. Baptista, M.A.; Miranda, J.M. Revision of the Portuguese catalog of tsunamis. *Nat. Hazards Earth Syst. Sci.* **2009**, *9*, 25–42. [CrossRef]
8. Hindson, R.A.; Andrade, C.; Dawson, A.G. Sedimentary processes associated with the tsunami generated by the 1755 Lisbon earthquake on the Algarve coast, Portugal. *Phys. Chem. Earth* **1996**, *21*, 57–63. [CrossRef]
9. Dawson, A.; Hindson, R.; Andrade, C.; Parish, R.; Bateman, M. Tsunami sedimentation associated with the Lisbon Earthquake of 1 November AD 1755: Boca do Rio, Algarve, Portugal. *Holocene* **1995**, *5*, 209–215. [CrossRef]
10. Scheffers, A.; Kelletat, D. Tsunami relics in the coastal landscape west of Lisbon, Portugal. *Sci. Tsunami Hazards* **2005**, *23*, 3–16.
11. Abrantes, F.; Lebreiro, S.; Rodrigues, T.; Gil, I.; Bartels-Jónsdóttir, H.; Oliveira, P.; Kissel, C.; Grimalt, J.O. Shallow-marine sediment cores record climate variability and earthquake activity off Lisbon (Portugal) for the last 2000 years. *Quat. Sci. Rev.* **2005**, *24*, 2477–2494. [CrossRef]
12. Abrantes, F.; Alt-Epping, U.; Lebreiro, S.; Voelker, A.; Schneider, R. Sedimentological record of tsunamis on shallow-shelf areas: The case of the 1969 AD and 1755 AD tsunamis on the Portuguese Shelf off Lisbon. *Mar. Geol.* **2008**, *249*, 283–293. [CrossRef]
13. Kennett, J. *Marine Geology*; Prentice-Hall: London, UK, 1982; p. 813.
14. Abrantes, F.; Rodrigues, T.; Montanari, B.; Santos, C.; Witt, L.; Lopes, C.; Voelker, A.H.L. Climate of the last millennium at the southern pole of the North Atlantic Oscillation: An inner-shelf sediment record of flooding and upwelling. *Clim. Res.* **2011**, *48*, 261–280. [CrossRef]
15. Hagelberg, T.; Pisias, N.; Shackleton, N.; Mix, A.; Harris, S. Refinement of a High-Resolution, Continuous Sedimentary Section for Studying Equatorial Pacific Ocean Paleoceanography, Leg 138. In *Proceedings of the Ocean Drilling Program: Scientific Results*; A&M University: College Station, TX, USA, 1995. [CrossRef]
16. Reimer, P.J.; Austin, W.E.N.; Bard, E.; Bayliss, A.; Blackwell, P.G.; Bronk Ramsey, C.; Butzin, M.; Cheng, H.; Edwards, R.L.; Friedrich, M.; et al. The IntCal20 Northern Hemisphere Radiocarbon Age Calibration Curve (0–55 cal kBP). *Radiocarbon* **2020**, *62*, 725–757. [CrossRef]
17. Heaton, T.J.; Köhler, P.; Butzin, M.; Bard, E.; Reimer, R.W.; Austin, W.E.N.; Bronk Ramsey, C.; Grootes, P.M.; Hughen, K.A.; Kromer, B.; et al. Marine20—The Marine Radiocarbon Age Calibration Curve (0–55,000 cal BP). *Radiocarbon* **2020**, *62*, 779–820. [CrossRef]
18. Blaauw, M. Methods and code for 'classical' age-modelling of radiocarbon sequences. *Quat. Geochronol.* **2010**, *5*, 512–518. [CrossRef]
19. Ramsey, C.B.; Dee, M.; Lee, S.; Nakagawa, T.; Staff, R.A. Developments in the Calibration and Modeling of Radiocarbon Dates. *Radiocarbon* **2010**, *52*, 953–961. [CrossRef]
20. Blaauw, M.; Christen, J.A. *Bacon Manual—v2. 3.9. 1*; School of Natural and Built Environment: Belfast, UK, 2013; pp. 1–13.
21. Stern, J.V.; Lisiecki, L.E. Termination 1 timing in radiocarbon-dated regional benthic δ18O stacks. *Paleoceanography* **2014**, *29*, 1127–1142. [CrossRef]
22. Yakupoğlu, N. Comparative Evaluation of Bayesian and Non-Bayesian AgeDepth Modelling Approaches: Bacon and Clam Approaches in Sediment Core Studies: Examples of Subaqueous environments from Türkiye. *Int. J. Environ. Geoinformatics* **2025**, *12*, 244–250. [CrossRef]
23. Wang, Y.; Goring, S.J.; McGuire, J.L. Bayesian ages for pollen records since the last glaciation in North America. *Sci. Data* **2019**, *6*, 176. [CrossRef] [PubMed]
24. Ausín, B.; Haghipour, N.; Wacker, L.; Voelker, A.H.L.; Hodell, D.; Magill, C.; Looser, N.; Bernasconi, S.M.; Eglinton, T.I. Radiocarbon Age Offsets Between Two Surface Dwelling Planktonic Foraminifera Species During Abrupt Climate Events in the SW Iberian Margin. *Paleoceanogr. Paleoclimatol.* **2019**, *34*, 63–78. [CrossRef] [PubMed]

25. Trachsel, M.; Telford, R.J. All age–depth models are wrong, but are getting better. *Holocene* **2017**, *27*, 860–869. [CrossRef]
26. Comas-Bru, L.; Rehfeld, K.; Roesch, C.; Amirnezhad-Mozhdehi, S.; Harrison, S.P.; Atsawawaranunt, K.; Ahmad, S.M.; Brahim, Y.A.; Baker, A.; Bosomworth, M.; et al. SISALv2: A comprehensive speleothem isotope database with multiple age–depth models. *Earth Syst. Sci. Data* **2020**, *12*, 2579–2606. [CrossRef]
27. Nanayama, F.; Shigeno, K.; Satake, K.; Shimokawa, K.; Koitabashi, S.; Miyasaka, S.; Ishii, M. Sedimentary differences between the 1993 Hokkaido-nansei-oki tsunami and the 1959 Miyakojima typhoon at Taisei, southwestern Hokkaido, northern Japan. *Sediment. Geol.* **2000**, *135*, 255–264. [CrossRef]
28. Newall, S.R.S.; Mackay, A.W.; Piotrowska, N.; Blaauw, M. A complete database of AMS radiocarbon estimates from Lake Baikal sediment cores with a lake-wide assessment of TOC age offsets. *Earth Syst. Sci. Data* **2026**, *18*, 1225–1242. [CrossRef]
29. Terrinha, P.; Noiva, J.; Brito, P.; Baptista, L.; Roque, C.; Drago, T.; Silva, P.; Magalhães, V.; Rodrigues, A.I.; Lopes, A. *Assessment, Strategy and Risk Reduction for Tsunamis in Europe*; Repositório Institucional: Lisbon, Portugal, 2017.
30. Feist, L.; Costa, P.J.M.; Bellanova, P.; Bosnic, I.; Santisteban, J.I.; Andrade, C.; Brückner, H.; Duarte, J.F.; Kuhlmann, J.; Schwarzbauer, J.; et al. Holocene offshore tsunami archive—Tsunami deposits on the Algarve shelf (Portugal). *Sed. Geol.* **2023**, *448*, 106369. [CrossRef]
31. Omira, R.; Baptista, M.A.; Matias, L.; Miranda, J.M.; Catita, C.; Carrilho, F.; Toto, E. Design of a Sea-level Tsunami Detection Network for the Gulf of Cadiz. *Nat. Hazards Earth Syst. Sci.* **2009**, *9*, 1327–1338. [CrossRef]
32. Wronna, M.; Omira, R.; Baptista, M.A. Deterministic approach for multiple-source tsunami hazard assessment for Sines, Portugal. *Nat. Hazards Earth Syst. Sci.* **2015**, *15*, 2557–2568. [CrossRef]
33. Baptista, M.A.; Miranda, J.M.; Chierici, F.; Zitellini, N. New study of the 1755 earthquake source based on multi-channel seismic survey data and tsunami modeling. *Nat. Hazards Earth Syst. Sci.* **2003**, *3*, 333–340. [CrossRef]
34. de Almeida, A.B. The 1755 Lisbon Earthquake and the Genesis of the Risk Management Concept. In *The 1755 Lisbon Earthquake: Revisited*; Mendes-Victor, L.A., Oliveira, C.S., Azevedo, J., Ribeiro, A., Eds.; Springer Netherlands: Dordrecht, The Netherlands, 2009; pp. 147–165.
35. Rodríguez-Vidal, J.; Cáceres, L.; Abad, M.; Ruiz, F.; González-Regalado, M.; Finlayson, C.; Finlayson, G.; Fa, D.; Rodríguez-Llanes, J.; Bailey, G. The recorded evidence of AD 1755 Atlantic tsunami on the Gibraltar coast. *J. Iber. Geol.* **2011**, *37*, 177–193. [CrossRef]
36. De Sousa, F.P. *O Terremoto do 1º de Dezembro de 1755 em Portugal. Um Estudo Demográfico. Distritos de Faro, Beja e Évora*; Tipografia do Comercio: Lisbon, Portugal, 1919.